

RESEARCH ARTICLE

Shearing overbite and asymmetrical jaw motions facilitate food breakdown in a freshwater stingray, *Potamotrygon motoro*

J. D. Laurence-Chasen^{1,2,*}, Jason B. Ramsay³ and Elizabeth L. Brainerd²**ABSTRACT**

Many species of fish process their prey with cyclic jaw motions that grossly resemble those seen in mammalian mastication, despite starkly different tooth and jaw morphologies. The degree of similarity between the processing behaviors of these disparate taxa has implications for our understanding of convergence in vertebrate feeding systems. Here, we used XROMM (X-ray reconstruction of moving morphology) to investigate prey processing behavior of *Potamotrygon motoro*, the ocellate river stingray, which has recently been found to employ asymmetrical, shearing jaw motions to break down its prey. We found that *P. motoro* modulates its feeding kinematics to produce two distinct types of chew cycles: compressive cycles and overbite cycles. The latter are characterized by over-rotation of the upper jaw relative to the lower jaw, past the expected occlusal limit, and higher levels of bilateral asymmetry as compared with compressive chews. We did not find evidence of the mediolateral shearing motions typical of mammalian mastication, but overbite cycles appear to shear the prey item between the upper and lower toothplates in a propalinal fashion. Additionally, comparison of hyomandibular and jaw motions demonstrates that the angular cartilages decouple jaw displacement from hyomandibular displacement in rostrocaudal and mediolateral directions. The multiple similarities between mammalian mastication and the dynamic processing behavior of *P. motoro* support the use of subfamily Potamotrygoninae as a model for studying evolutionary convergence of mastication-like processing.

KEY WORDS: XROMM, Kinematics, Chewing, Mastication, Prey processing, Modulation

INTRODUCTION

Food processing is a vital stage in feeding. Through crushing, grinding and shearing motions of the teeth and jaws, gnathostome vertebrates can dramatically increase the surface area of a prey item and maximize the ultimate energetic reward of a feeding event (Farrell, 1956; Lucas et al., 2002; Reilly et al., 2001). When these jaw motions are cyclic and performed repeatedly on an intraoral prey item, the behavior is termed chewing (Ross and Iriarte-Diaz, 2014). The study of chewing has traditionally focused on mammals, whose temporomandibular joint and heterodont dentition facilitate asymmetrical motions and transverse or propalinal shear forces

(Herring, 1993; Menegaz et al., 2015). The evolution of this masticatory apparatus is thought to have played a role in the rapid diversification of early mammals (Crompton and Parker, 1978; Luo, 2007; Turnbull, 1970). However, mammals are not the only animals who chew. Many fishes use cyclic oral or pharyngeal jaw movements to chew their food prior to swallowing (Bemis and Lauder, 1986; Gidmark et al., 2014; Gintof et al., 2010; Lauder, 1980). But do fish chew like mammals? Most studies of fish feeding have focused on prey capture, rather than processing, and thus the degree to which fish and mammals have converged on similar processing behavior is unclear.

The batoids (rays, skates, guitarfishes and sawfishes) consume a range of hard and tough prey and are known for their elaborate prey processing strategies (Dean et al., 2005, 2007; Kolmann et al., 2016; Sasko et al., 2006; Wilga and Motta, 1998). Notably, their cranial anatomy differs from that of teleost fishes, as they lack pharyngeal jaws, and from that of other elasmobranchs in that they exhibit a euhystylic jaw suspension, wherein all skeletal and ligamentous connections between the upper jaw (palatoquadrate) and the cranium have been lost (Maisey, 1980; Wilga, 2002). The palatoquadrate and lower jaw (Meckel's cartilage) are suspended solely by rod-like cartilages, the paired hyomandibulae, that articulate with the caudolateral surface of the chondrocranium (Fig. 1). Relative to other jaw suspension systems, euhystyly is thought to permit a greater range of upper and lower jaw motions during feeding (Dean and Motta, 2004a; Dean et al., 2005; Wilga and Motta, 1998).

One group of freshwater stingrays, the sub-family Potamotrygoninae, has recently received attention for its complex prey processing kinematics and derived hyomandibular morphology (Kolmann et al., 2016). Potamotrygonins are the neotropical, obligate freshwater members of the family Potamotrygonidae, to which the genus *Styracura* has recently been added (Carvalho et al., 2016). In most batoids, the hyomandibulae articulate directly with the lateral aspect of the Meckel's cartilage; yet in many potamotrygonins the joint is bridged by one or more small angular cartilages (Fig. 1; Lovejoy, 1996). Fontenelle et al. (2017) provide a comprehensive description of the diversity in angular cartilage morphology across Potamotrygoninae, as well as propose several functional hypotheses that we test in the present study. Specifically, they suggest that angular cartilages act as out-levers to extend the range and protrusive velocity of the jaws, and that the addition of a second cartilage braces the jaw joints during the processing of hard and tough prey. *Potamotrygon motoro*, the subject of this study, possesses two angular cartilages on each side of the head (Fig. 1), which we refer to as the anterior angular cartilage (AAC) and the posterior angular cartilage, *sensu* Fontenelle and colleagues (2017). We predict that the elongate morphology of *P. motoro*'s AAC enables the jaws to protrude further and faster from the head than the distal ends of the hyomandibulae, and that the 3D motions of the jaws relative to the hyomandibulae will be limited by the bracing effect of the two cartilages.

¹Department of Organismal Biology and Anatomy, The University of Chicago, 1027 E 57th St, Chicago, IL 60637, USA. ²Department of Ecology and Evolutionary Biology, Brown University, 80 Waterman Street, Providence, RI 02912, USA.

³Biology Department, Westfield State University, 577 Western Avenue, Westfield, MA 01086, USA.

*Author for correspondence (jdlaurance@uchicago.edu)

✉ J.D.L., 0000-0001-6192-175X; E.L.B., 0000-0003-0375-8231

Received 4 December 2018; Accepted 10 June 2019

List of symbols and abbreviations

AAC	anterior angular cartilage
ACMH	chondrocraniohyomandibular articulation
ACS	anatomical coordinate system
DoF	degree of freedom
JCS	joint coordinate system
QMJ	quadratomandibular joint
R_x	rotation about the x-axis
R_y	rotation about the y-axis
R_z	rotation about the z-axis
XROMM	X-ray reconstruction of moving morphology

Kolmann et al. (2016) used high-speed video to investigate the processing kinematics of *P. motoro*. By varying prey type, they found that *P. motoro* chews with more frequent symphyseal flexion and asymmetrical shearing motions when a prey item is tougher. Asymmetry, shearing and modulation based on sensory feedback are hallmarks of mammalian chewing (Ross et al., 2007). In the case of mammals, bilateral asymmetry is 'active', in the sense that it is the result of differential neuromuscular activity (Hiiemae, 1978). Asymmetrical muscle activation driving asymmetrical hyomandibular depression and jaw protrusion has been found in batoids (Dean and Motta, 2004b; Gerry et al., 2010; Wilga and Motta, 1998). But it is unclear whether the symphyseal flexion and asymmetry noted by Kolmann et al. (2016) are necessarily the result of active modulation or passive prey forces. In fact, there seem to be at least two distinct types of asymmetry outlined in the literature: Gerry and colleagues (2010) describe whole-jaw deviation from the

midline during mouth opening, and Kolmann and colleagues (2016) suggest relative shearing of the upper and lower jaws during occlusion. Experimental measurement and disambiguation of these translations and rotations have been hindered by the ventral position of the mouth and the large amount of labial tissue that obscures most of the cranial cartilages and articulations from an external view.

To visualize and quantify the translations and rotations of the cranial cartilages in *P. motoro*, we used XROMM (X-ray reconstruction of moving morphology) to produce accurate 3D animations of the chondrocranium and the left and right hyomandibulae, palatoquadrate cartilages and Meckel's cartilages (Fig. 1). We provide 3D kinematic descriptions of prey processing behaviors and compare the bilateral displacements of the hyomandibulae and jaws to test the recent functional hypotheses of angular cartilage function, asymmetrical jaw motions and similarities with mammalian chewing.

MATERIALS AND METHODS

This study investigates the prey processing kinematics of three ocellate river stingrays, *Potamotrygon motoro* (Müller and Henle, 1841) ($N=3$, disk widths 150, 180 and 250 mm). The stingrays were purchased from Aquascape Online (Belleville, NJ, USA) and Ocean State Aquatics (Coventry, RI, USA) and were housed in 250 liter aquaria. Animals were fed a variety of commercially available elasmobranch food. Experimental prey comprised odonate larvae and beef heart embedded with one or two 1.0 mm spherical metal beads that allowed intraoral location. All surgical and experimental techniques were approved by Brown University's Institutional Animal Care and Use Committee, protocol number 1509000157.

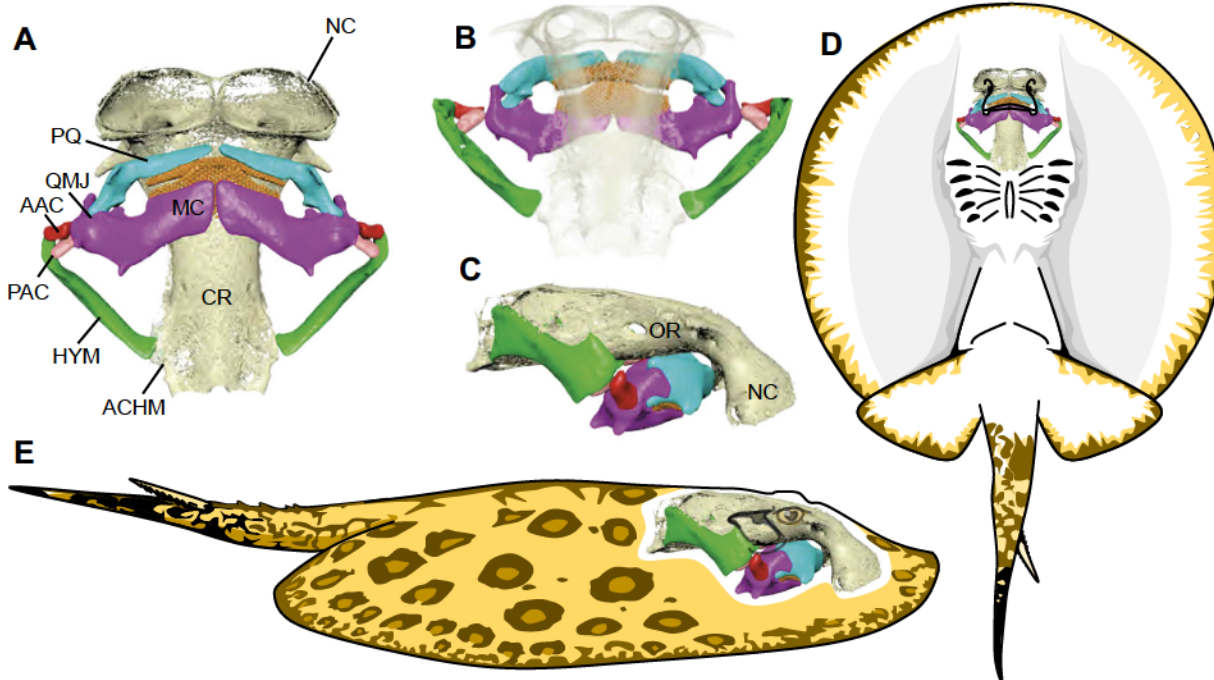


Fig. 1. Cranial anatomy of *Potamotrygon motoro*. Paired hyomandibulae (green) suspend the palatoquadrate (cyan) and Meckel's cartilage (magenta) from the chondrocranium (beige) via two small angular cartilages. The anterior angular cartilage (red) is slightly larger and more mineralized than the posterior angular cartilage (light red). Note the lack of a direct connection between the upper jaw (palatoquadrate) and chondrocranium, the defining feature of the batoid euhostylic jaw suspension. (A) Ventral view. (B) Caudodorsal view with semi-transparent chondrocranium. (C) Left lateral view. Mesh models generated from a microCT scan. (D) Ventral and (E) lateral views of whole ray, showing skeletal positions relative to the body. AAC, anterior angular cartilage; ACHM, chondrocraniohyomandibular articulation; CR, chondrocranium; HYM, hyomandibula; MC, Meckel's cartilage; NC, nasal capsule; OR, orbit; PAC, posterior angular cartilage; PQ, palatoquadrate; QMJ, quadratomandibular joint. For scale, the chondrocranium in this individual was 65 mm long.

Marker implantation, data collection and processing

We used marker-based XROMM to create 3D animations of *P. motoro*'s major cranial cartilages during feeding. A detailed description of XROMM is available in a previous publication (Brainerd et al., 2010) and online at www.xromm.org. Here, we surgically implanted, under anesthesia (buffered tricaine methanesulfonate, $0.075\text{--}0.095\text{ g l}^{-1}$), three to five conical tungsten carbide markers (Kambic et al., 2014) into the chondrocranium, palatoquadrate, Meckel's cartilage and hyomandibulae. One individual (Pm03) did not receive hyomandibular markers. Markers were implanted bilaterally to measure potential asymmetry and to quantify motion at the jaw symphyses. After marker implantation, we injected an analgesic (butorphanol, 0.04 mg kg^{-1}), and allowed at least 7 days for the animal to recover before recording. We found elasmobranch cartilage to be well suited for the conical marker implantation technique detailed in Kambic et al. (2014). The conical markers were approximately 1 mm long and allowed for percutaneous implantation without incising or drilling. The conical markers showed up clearly in the X-ray videos (Movie 1), and tracked well with a mean precision of $0.054\pm 0.003\text{ mm}$ (mean \pm s.e.m. of the standard deviations of pairwise marker to marker distances for all markers within rigid bodies, with $n=85$ marker pairs).

To increase motivation, food was withheld for at least 24 h before video recording. We avoided the potentially stressful transfer to a 'recording tank', and instead moved the animals in their long-term aquarium into the X-ray room the night before recording. X-ray videos were collected with custom-made biplanar videoradiography equipment (Miranda et al., 2011). Videos were 10 s long, 200 frames s^{-1} , with an X-ray technique of 95–100 kV, and 150–200 mA. Standard, external view videos were synchronously recorded with a GoPro Hero 3 (GoPro, San Mateo, CA, USA) at 120 frames s^{-1} to provide external reference images for the entire processing sequence. All videos are stored on the XMAPortal (xmaportal.org, permanent ID BROWN57) in accordance with best practices for video data management in organismal biology (Brainerd et al., 2017).

After a full dataset (≥ 10 trials per individual) was collected, animals were euthanized with an overdose of tricaine methanesulfonate and their heads were scanned with a SkyScan 1173 microCT scanner at the Karel F. Liem Imaging Facility (University of Washington, Friday Harbor Laboratories, WA, USA) with an aluminium filter, 1000 pixel image size and 50–60 μm voxels. Individual cartilage models were segmented in Horos (horosproject.org) and smoothed in Geomagic Studio 2014 (3D Systems, Rock Hill, NC, USA). Camera calibration images and X-ray videos were processed in the open-source software XMALab (Knörlein et al., 2016, bitbucket.org/xromm/xmalab). We used XMALab to undistort X-ray videos, calculate the 3D camera positions, and track markers. After importing the marker coordinates from the microCT scan, XMALab calculated the rigid body motion of each cartilage and filtered those transformations with a 25 Hz low-pass Butterworth filter. Then, in Maya 2017 (Autodesk, San Rafael, CA, USA), we applied the transformations to the cartilage models to create XROMM animations. After data were exported from Maya, all analyses were performed in MATLAB (R2017a, MathWorks, Natick, MA, USA).

Joint coordinate systems

To measure the motion of individual cartilages relative to other cartilages, we used joint coordinate systems (JCSs), implemented in Maya with the open-source package XROMM MayaTools (bitbucket.org/xromm/xromm_mayatools). A JCS comprises two anatomical coordinate systems (ACSs). By attaching one ACS to a

proximal element and another to a distal element, we can measure the relative rotations (Euler angles) and translations of the elements, for a total of six degrees of freedom (DoF) per joint. Euler angles were calculated in Autodesk Maya with the rotation order ZYX, with polarity determined by the right-hand rule with the thumb pointing in the direction of the arrow on each axis.

We placed JCSs at six joints: two joints bilaterally, the chondrocraniohyomandibular articulation (ACHM) and quadratomandibular joint (QMJ, or 'jaw joint'), and at the midline symphyses between the left and right Meckel's cartilages and palatoquadrates (Fig. 2). The symphysis JCSs were placed midline between the two hemi-cartilages of the upper and lower jaw, and measured the motion of the right hemi-cartilage relative to the left hemi-cartilage (Fig. 2C,D). We predicted, *a priori*, that the majority of symphyseal rotation would occur about the anatomical line of the symphysis. Accordingly, we oriented the Z-axis of the palatoquadrate and Meckel's cartilage symphysis JCSs along the long axis of the symphyses. Because the Meckel's cartilage and palatoquadrate symphyses are oriented differently relative to the chondrocranium (rostrocaudal versus dorsoventral, respectively), the symphysis JCSs are offset by approximately 90 deg.

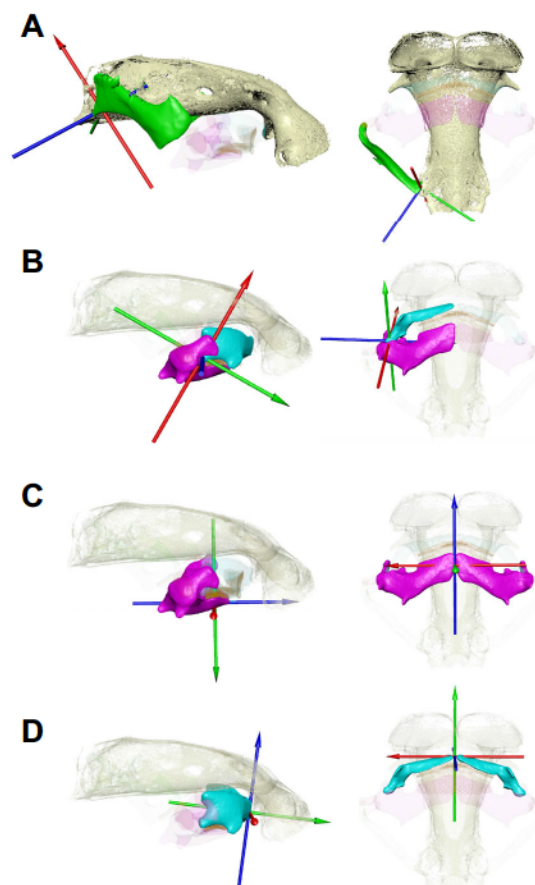


Fig. 2. Joint coordinate system (JCS) orientations.
 (A) Chondrocraniohyomandibular articulation (ACHM). (B) Quadratomandibular joint (QMJ). (C) Meckel's cartilage symphysis. (D) Palatoquadrate symphysis. The QMJ JCS measures motion of the Meckel's cartilage relative to the palatoquadrate. The symphysis JCSs measure the motion of the right hemi-cartilage relative to the left hemi-cartilage. In each joint, the blue axis is Z, the primary rotational axis; the red axis is X; and the green axis is Y. Only the right side is shown here, but JCSs were placed bilaterally for the QMJ and ACHM. For these bilateral measurements, JCSs were oriented such that the polarity of the Z- and Y-axes for a given motion remained the same.

In keeping with conventional measures of jaw depression (e.g. Menegaz et al., 2015), the QMJ JCSs measured the motion of Meckel's cartilage relative to the palatoquadrate, with the Z-axis oriented mediolaterally (Fig. 2B). Systematic alteration of this orientation confirmed that this configuration best isolated the motion at the joint to a single axis. The Y-axis was oriented such that, in a sagittal view, it ran from the joint to the labial surface of the cartilage toothplate. The expected occlusal limit was the zero of the Z-axis rotation – or when the labial surfaces of the upper and lower toothplates first make contact. Importantly, each QMJ JCS captured motion at the joint that resulted from both Meckel's cartilage and palatoquadrate rotation, and did not differentiate between the two. Thus, in order to measure the relative contribution of Meckel's cartilage and palatoquadrate rotation to gape closure, we also measured the rotation of each cartilage relative to the chondrocranium. For the two bilateral joints, data shown in the present study came from the right joint, unless otherwise noted.

Temporal measurements

Chew cycles were defined as maximum gape to maximum gape. Local maxima and minima were identified by visual inspection of the Z-axis rotation trace of the QMJ. Owing to heat buildup in the X-ray tube, X-ray videos were limited to a maximum duration of 10 s, and thus the total duration of each processing sequence was measured from the external GoPro videos. The coefficient of variation (CV) of cycle duration was calculated following Sokal and Braumann (1980), in which $CV = [1 + (1/4n)] \times (s/Y)$, where n is the sample size, s is the standard deviation and Y is the sample mean.

Landmark displacements

We used digital landmarks (Fig. 3) to test hypotheses about the role of the angular cartilages, quantify shearing motions, and quantify bilateral asymmetry. In each case, a locator was created in Autodesk Maya and was rigidly attached so it moved with the animated

cartilage model of interest. Then we used MayaTools to calculate the displacement of the locator in the frame of reference of an ACS attached to the reference element.

The two landmarks used in angular cartilage measurements were the AAC's attachment sites: the distal end of the hyomandibula and the lateral face of the Meckel's cartilage (Fig. 3A). Their motion was measured relative to the chondrocranium. We inferred that any difference in motion represents the functional contribution of the angular cartilages. In order to quantify differences in motion, we first calculated the Pearson linear correlation coefficient of the landmarks' instantaneous velocity in each translational DoF, across all cycles. The calculation results in a unitless number that represents the degree of linear dependence of one variable (hyomandibula landmark velocity) on the other variable (Meckel's cartilage landmark velocity). A correlation coefficient of zero suggests no relationship, which is unlikely in a biomechanical linkage. Values of 1 or -1 are perfect positive and negative correlations, respectively. The former would indicate that the two landmarks are moving exactly together, i.e. rigidly connected. To test whether the angular cartilages increase the protrusive velocity of the jaws, we also performed two-tailed *t*-tests (alpha=0.01) on the average protrusive speed (no direction) of the two landmarks during 14 jaw protrusions. Average protrusion speed was calculated as the linear distance between the XYZ position of the landmark at the start of protrusion and maximum protrusion, divided by time.

Shearing was quantified by measuring the displacement of the midline palatoquadrate toothplate relative to an ACS at the same location on the Meckel's cartilage toothplate (Fig. 3B). As the toothplates themselves were not individually animated, they were treated as rigid extensions of their underlying cartilages. Batoid toothplates do not act as rigid bodies (Dean et al., 2008), so we limited our use of information from the toothplate models to the approximate locations of their surfaces. Whole-jaw deviation from the midline was quantified by measuring the mediolateral displacement of a landmark on the medial border of the right Meckel's cartilage relative to the cranium.

Analysis of jaw kinematics

Mean per-cycle joint rotations (Table S3) were calculated in two ways. First, in a path-independent manner, the mean difference in rotation magnitude at maximum gape and minimum gape was taken across all cycles. Second, to account for joint motions that are not captured by the first method, we summed the absolute value of the difference in rotation magnitude between each consecutive frame from maximum gape to minimum gape, then calculated the mean sum of differences across all cycles.

We used two-sample *t*-tests (alpha=0.01, two tails) to compare jaw kinematics during overbite cycles with a set of randomly selected compressive cycles. Tests were performed on the change in angle or position from maximum to minimum gape for measured kinematic variables (Table 1). For a subset of variables (ACHM rotation, QMJ rotation and Meckel's cartilage X-axis rotation, R_x), the difference in magnitude between the left and right sides were compared to test for the presence of bilateral asymmetry during overbites. In the case of the Meckel's cartilage R_x , any non-zero rotation constitutes greater asymmetry.

In addition, a principal component analysis (PCA) was conducted to assess the key drivers of cycle-to-cycle variation in the dataset. The input to the analysis was the change in angle from maximum gape to minimum gape for all measured rotational degrees of freedom. A complete list of variables and resultant loadings is provided in Table S1.

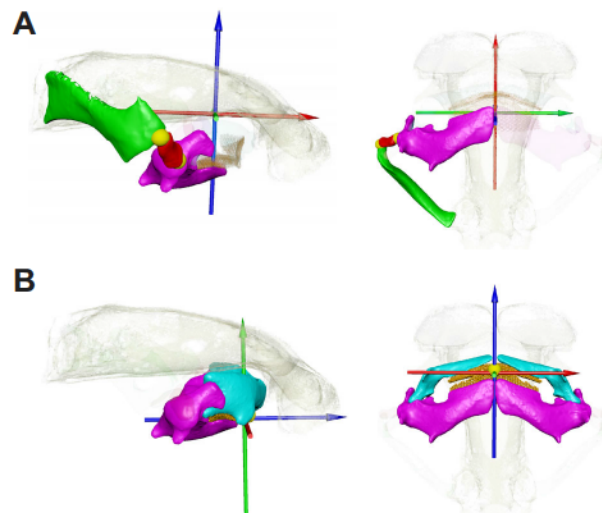


Fig. 3. Digital landmarks and anatomical coordinate system (ACS) orientations. (A) To quantify the functional role of the angular cartilages, the displacement of digital landmarks (yellow spheres) representing the proximal and distal attachment sites of the anterior angular cartilage were measured relative to the chondrocranium. The chondrocranium ACS was placed in standard anatomical orientation. (B) Palatoquadrate landmark used to track motion of palatoquadrate relative to an ACS attached to Meckel's cartilage. Note that the orientation of the ACS will vary with pose of Meckel's cartilage.

Table 1. Results of significance tests (*P*-values) comparing kinematics of overbite and compressive chew cycles

Variable	Degree of freedom		
	X	Y	Z
ACHM rotation	0.043	0.604	0.752
QMJ rotation	<0.001	0.007	<0.001
Shearing landmark displacement	0.021	<0.001	<0.001
QMJ rotation bilateral asymmetry	0.035	0.005	<0.001
ACHM rotation bilateral asymmetry	0.139	0.065	0.069
Meckel's cartilage symphysis rotation	<0.001*	0.431	0.156
Palatoquadrate symphysis rotation	0.265	0.025	0.290

ACHM, chondrocraniohyomandibular articulation; QMJ, quadratomandibular joint. *Symphysial twisting is, by definition, bilateral asymmetry.

Precision study

An XROMM precision study for 6-DoF JCS motion was conducted following the methods of Menegaz et al. (2015). In brief, after euthanization, individual Pm05 was frozen and waved in the X-ray capture volume at the approximate frequency of the behavior (3 Hz). This 'frozen wave' was recorded with the same parameters (e.g. water depth, X-ray machine configuration and settings) used for *in vivo* data collection. Five-hundred frames of the cadaveric trial were taken through the XROMM processing workflow, and the standard deviation of each DoF of each JCS and ACS measurement was taken. Because there should be no movement within the joints of the frozen specimen, these standard deviations represent the precision threshold of the study. The results of the precision study are provided in Table S2, and demonstrate that the precision thresholds of rotations (range 0.160–0.916 deg) and translations (range 0.018–0.204 mm) were consistent and small relative to the motions we report from our live stingrays.

RESULTS

XROMM and standard light video confirmed that *P. motoro* processes its prey with rapid, cyclic chews (Movie 2). All three individuals chewed at similar frequencies with a mean of 3.38 ± 0.22 Hz (here and elsewhere, reported means are the combined mean of means for 67–80 cycles per individual \pm s.e.m., $n=3$ individuals) and for similar overall train durations (15.3 ± 1.4 s). The

mean CV of chew cycle duration was $31.4 \pm 2.2\%$. Throughout the processing sequences, the cartilaginous elements of the feeding apparatus were highly kinetic.

Suspensory apparatus kinematics

Cyclic depression and elevation of the hyomandibulae during prey processing resulted from rotation (*R*) at the ACHM. Consistent with its hinge-like morphology (Fig. 1A,B), the majority of ACHM rotation was concentrated about a single axis, ACHM R_z (Fig. 4). Positive ACHM R_z (depression) was usually bilaterally symmetric and caused the jaws to protrude ventrally and slightly rostrally and medially relative to the chondrocranium. Notably, during some capture and mid-sequence recapture events (i.e. after the prey had fallen out of the mouth), the left and right hyomandibulae depressed differentially. In these cases, asymmetrical hyomandibular depression caused the jaws to deviate from midline and protrude to the left or right side. Peak positive ACHM R_z values co-occurred with the largest gape maxima (Fig. 4, asterisks), when prey was being transported from outside to inside the mouth or from between the toothplates to the back of the mouth.

We compared the motion of the AAC proximal and distal attachment sites relative to the chondrocranium to determine the functional role of the angular cartilages (see Materials and Methods, Landmark displacement). The degree of dissimilarity between the velocity of the two landmarks depended on the direction of motion (Fig. 5). Along a dorsoventral axis, the landmarks' velocity was highly correlated, with a Pearson correlation coefficient of 0.925 ± 0.004 ($\pm 99\%$ confidence interval). However, the correlation dropped to 0.65 ± 0.2 and 0.53 ± 0.02 along the rostrocaudal and mediolateral axes, respectively. To test the hypothesis that the angular cartilages increase the protrusive velocity of the jaws relative to the hyomandibulae, we compared the linear speed of the two landmarks during 14 rapid jaw protrusions. We found no significant difference (two-tailed *t*-test, $P=0.93$) between the mean speed of the landmarks. But, despite the same speed, a per-axis breakdown of the landmarks' velocities during protrusion showed directional differences. Specifically, the hyomandibula landmark's medial velocity component was on average greater ($P=0.003$), whereas the opposite was true for rostral motion, where the

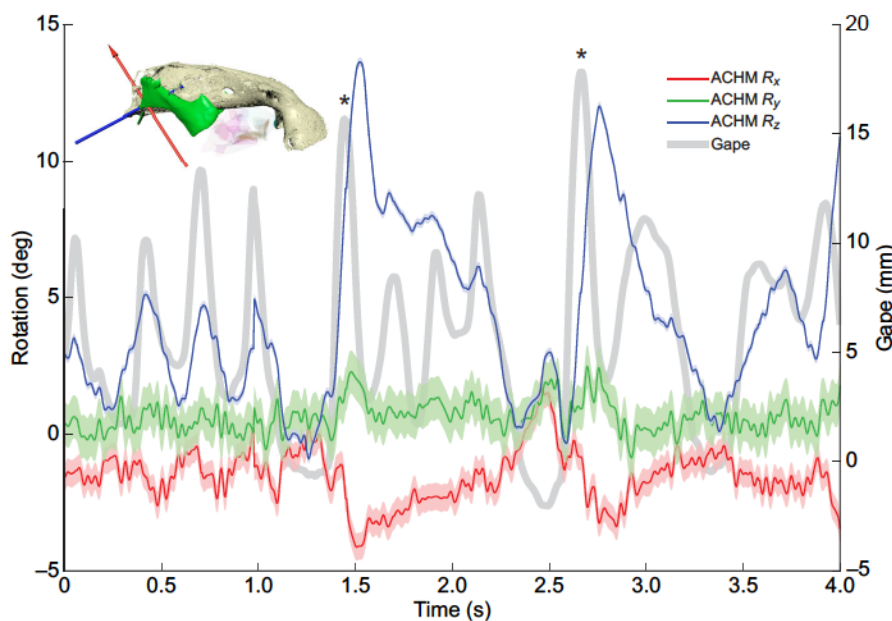


Fig. 4. Chondrocraniohyomandibular articulation (ACHM) kinematics. JCS rotation data show X, Y and Z rotations with noise thresholds during a representative 4-s processing sequence in Pm05. The majority of rotation is concentrated about the Z-axis, consistent with the hinge-like appearance of the joint. While there is motion throughout processing, we see the highest peaks in R_z coincide with the largest peak gapes (*); corresponding to mid-processing re-capture and transport events.

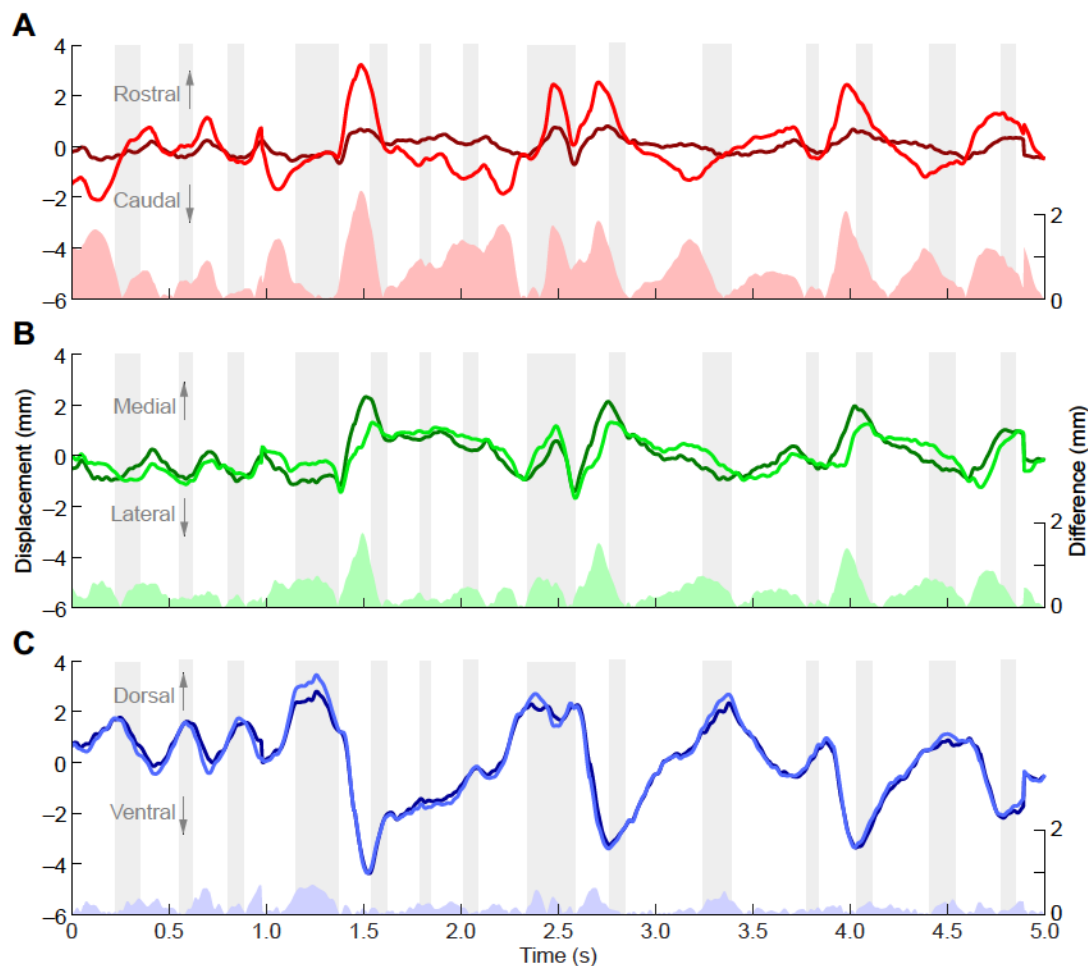


Fig. 5. Functional role of the angular cartilages. The traces represent the mean-subtracted displacement of the proximal (darker lines) and distal (lighter lines) attachment sites of the anterior angular cartilage on the hyomandibula and Meckel's cartilage, respectively. The solid-filled traces at the bottom of each panel show the difference in displacement between the attachment sites. Gray shaded regions represent the occlusal phase of each chew cycle. (A) Rostrocaudal displacement, where positive is rostral. (B) Mediolateral displacement, where positive is medial. (C) Dorsoventral displacement, where positive is dorsal. Note that the largest difference occurs along a rostrocaudal axis, whereas the motion of the two landmarks along a dorsoventral axis is remarkably similar. Thus, the angular cartilages permit decoupling hyomandibular motion from jaw motion in a direction-dependent manner. Data are from a representative 5-s processing sequence in individual Pm05.

Meckel's cartilage landmark had a greater velocity ($P=0.009$). Or, in other words, the distal ends of the hyomandibulae came together toward the midline, while the jaws went forward, both at the same speed.

Jaw kinematics

We observed substantial rotations at all of *P. motoro*'s jaw joints: the QMJ, palatoquadrate symphysis and Meckel's cartilage symphysis. The majority of QMJ rotation occurred about a mediolateral axis, QMJ R_z , and was the result of both upper and lower jaw rotation relative to the chondrocranium. The relative contribution of palatoquadrate and Meckel's cartilage rotation to gape closure varied substantially cycle-to-cycle, but on average, $57.2\pm12.2\%$ of mouth closure was due to palatoquadrate rotation. Overall, the QMJ exhibited a remarkable range of motion. The functional range of rotation about the X -, Y - and Z -axes was 13.6 ± 0.93 , 25.1 ± 1.15 and 104.7 ± 3.63 deg, respectively (see Fig. 2B for axis orientations).

The jaw symphyses of *P. motoro* were extremely flexible and exhibited substantial rotations (Movie 2). Unlike in the ACHM

and QMJ, the motion captured by the anatomically informed JCSs was not concentrated about any one axis, and instead was approximately evenly split among the three: rotation along the midline of the symphysis (R_z), flexion that decreases the resting angle between the hemicartilages (R_y), and twisting of the left and right hemicartilages relative to each other (see Fig. 2C,D for axis orientations). The palatoquadrate symphysis showed a rotational range of motion of 29.0 ± 4.0 , 23.8 ± 3.2 and 25.6 ± 1.4 deg about the X -, Y - and Z -axes, respectively. The Meckelian symphysis range of motion was similarly 37.9 ± 2.1 , 29.3 ± 3.7 and 30.1 ± 5.0 deg. Mean joint rotations for each DoF are provided (Table S3). We found that a path-independent, gape-based calculation of rotation does not fully capture the substantial rotations that occur at the upper and lower jaw symphyses throughout the gape cycle.

Two types of chew cycles

In order to assess the presence of shearing motions, we measured the displacement of a landmark on the palatoquadrate relative to the Meckel's cartilage. For the majority of cycles, the palatoquadrate landmark reversed direction at, or prior to, the expected occlusal

limit (Fig. 6A). Visual inspection of prey position via prey markers confirmed that during these cycles, the prey was between the jaws. Thus, we termed these cycles compressive cycles. There was no evidence of transverse or propalinal shearing during compressive cycles. However, we noted that *P. motoro* would occasionally perform what appeared to be a kinematically distinct behavior, in which the palatoquadrate continued well past the expected occlusal limit (Fig. 6, blue lines). Accordingly, we termed these events 'overbite cycles'. During overbite cycles, the palatoquadrate rotates down more than is typical, and shears the prey along the curved path of the Meckel's cartilage toothplate, in a propalinal fashion (Movie 3). Overbite cycles were often followed by a cycle that involved rapid, intraoral reorientation of the prey item. We did not find any mediolateral translation of the palatoquadrate relative to the Meckel's cartilage during compressive or overbite cycles in our

individuals feeding on the food types provided (beef heart and odonate larvae).

To assess the main drivers of variation in the dataset and to test whether overbite cycles are indeed a separate behavior, we performed a PCA on the change in angle (maximum gape to minimum gape) for every rotational DoF, for every chew cycle (Fig. 7). Cycles were coded as compressive or overbite *a priori*, based on their gestalt appearance in plots such as those in Fig. 6. The analysis shows distinct clusters of compressive cycles and overbite cycles when visualized in PC space. This provides further evidence that there is a kinematic difference between cycle types. Importantly, PCA allowed us to identify bilateral jaw joint rotation ($QMJ R_z$) and Meckel's cartilage symphysis twisting ($MC R_x$) as the top three contributors to the variation along the first PC, where the separation between compressive chews and overbites is

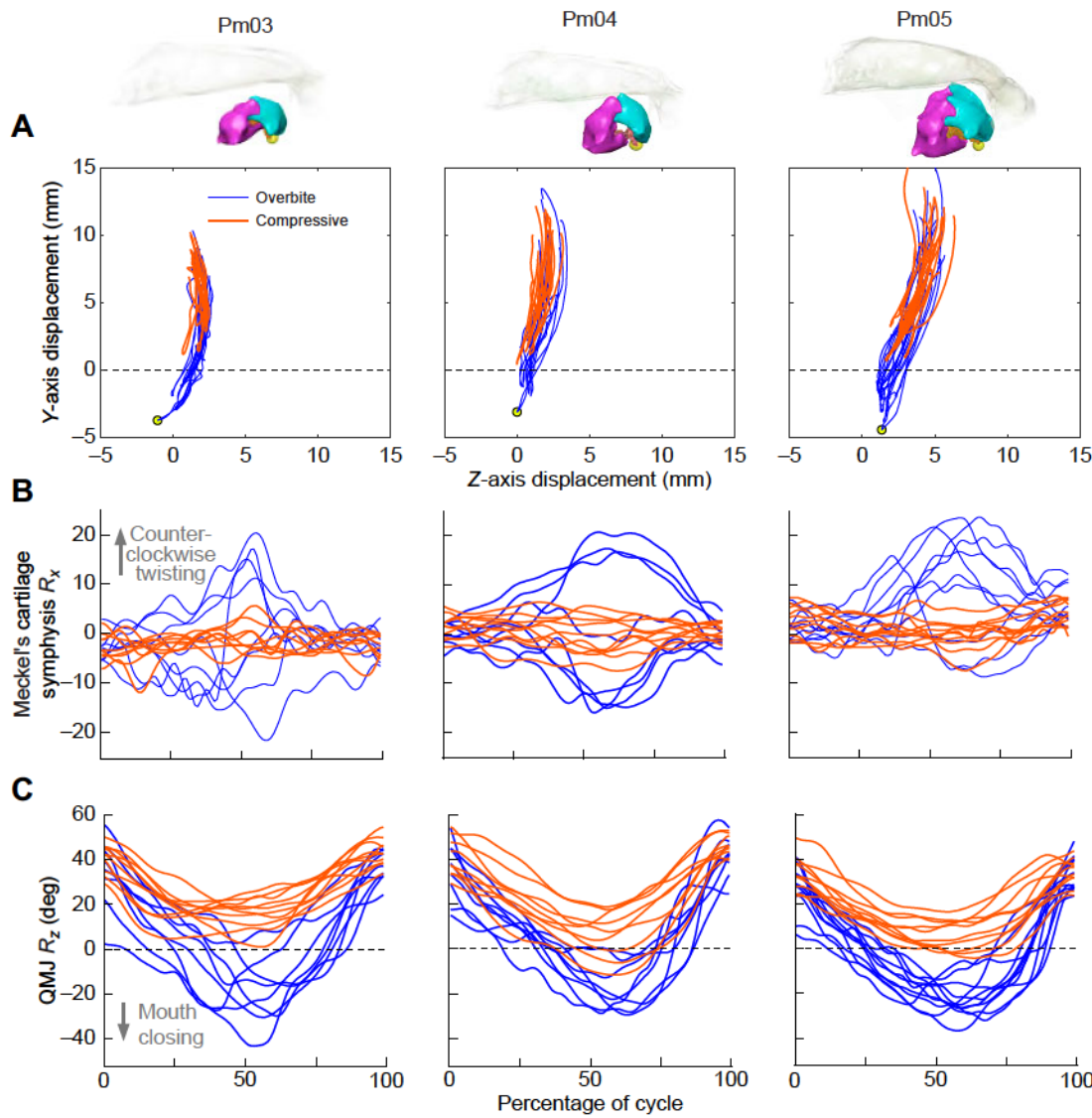


Fig. 6. Kinematic comparison of overbite and compressive chew cycles in three *P. motoro* individuals. (A) In both compressive cycles (orange) and overbite cycles (blue), a landmark midline on the palatoquadrate (yellow sphere) is displaced relative to an ACS midline on the Meckel's cartilage (Fig. 3B). However, during overbite cycles, the displacement is significantly larger ($P<0.001$, one-tailed t -test), passing the expected occlusal limit (dashed line). The added displacement shears the prey between the palatoquadrate and Meckel's cartilage toothplates, in a midsagittal plane. (B) Twisting at the Meckel's cartilage symphysis (rotation about the red X-axis in Fig. 2C) was significantly greater during overbites ($P<0.001$, one-tailed t -test). Counterclockwise rotation is defined as right Meckel's cartilage relative to left, viewed from the left side. (C) QMJ rotation (about the blue Z-axis in Fig. 2B) was also greater during overbites, producing the observed displacement past the occlusal limit (dashed line).

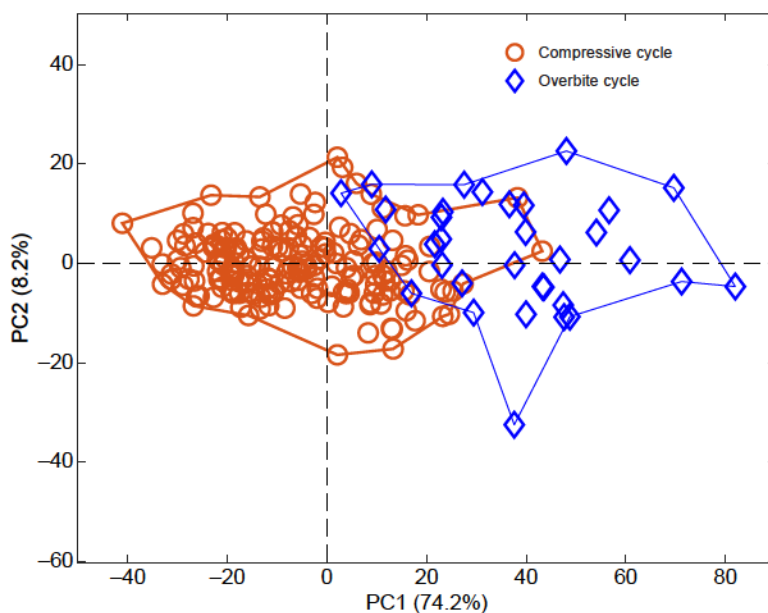


Fig. 7. Principal component analysis (PCA) of joint rotations. Each symbol represents a chew cycle for which the difference between maximum and minimum rotation magnitudes within that cycle were calculated. All rotational degrees of freedom (six joints) were included. Cycles were coded, *a priori*, as either compressive (circles) or overbite (diamonds) cycles. The first PC captures the majority of the variation, and is dominated by quadratomandibular joint Z-axis rotation. Note that zero is at the center of the compressive cycle cluster.

seen. Indeed, we found that overbites are characterized by exaggerated QMJ R_z (Fig. 6C), as well as MC R_x values (Fig. 6B).

Asymmetry

We found clear bilateral asymmetry in the rotation of multiple joints (Fig. 8). As described above, the ACHM occasionally exhibited unilateral depression, resulting in whole-jaw deviation to one side (Fig. 8C,D). The overbite cycles also showed substantial asymmetrical components. Often during an overbite, one of the QMJs would exhibit more negative Z-axis rotation, i.e. one side of the mouth would close more (Fig. 8A). As noted above, we observed substantial X-axis rotation at the Meckel's cartilage symphysis during overbites, indicating independent motion of the left and right Meckel's cartilages (Figs 8B and 6B). Statistical tests confirmed that there is significantly ($P<0.01$) more asymmetry during overbite cycles than during compressive cycles for several kinematic variables (Table 1). To investigate whether the asymmetry was the result of passive prey forces or active modulation, we identified the location of the prey within the jaws during a subset of 20 cycles with the greatest bilateral asymmetry in QMJ R_z . In nine of these cycles, the prey item was on the side of the jaws that closed down more.

DISCUSSION

Our results show that *P. motoro*'s euhyostylic jaw suspension facilitates asymmetrical jaw motions and two kinematically distinct types of chewing cycles: compressive chews and shearing overbite chews. Anatomical specializations including elongate hyomandibulae, and extra joints added to the system by the presence of angular cartilages allow tremendous freedom for the jaws to translate and rotate asymmetrically relative to the chondrocranium. In some chewing cycles, the hyomandibulae rotated by unequal amounts at their joints with the chondrocranium, directing the jaws to protrude and retract asymmetrically (Fig. 8). In other chewing cycles, we discovered that the palatoquadrate rotates well past normal occlusion to slide along the curved surface of the lower toothplate and shear the prey between the two toothplates (Fig. 6). These overbite cycles are distinct from the more common compressive chewing cycles and are facilitated by flexibility at both the Meckelian and palatoquadrate symphyses and the euhyostylic

freedom of the palatoquadrate from any direct connection to the chondrocranium.

Role of the hyomandibulae

The hyomandibulae suspend the jaws and their motion is thought to guide the direction of jaw protraction and depression in batoids (Dean et al., 2007; Kolmann et al., 2014). Our data confirm that hyomandibular depression is closely correlated with jaw depression (Fig. 4), and that asymmetrical hyomandibular motion guides the jaws to protrude asymmetrically (Fig. 8). As was predicted from morphological observation, motion at the ACHM is hinge-like (Fig. 1), i.e. concentrated mainly about a single axis (Fig. 4). Notably, the range of motion about the major rotational axis (16 deg) was smaller than the hyomandibular rotations that have been described or inferred in other elasmobranchs (Dean and Motta, 2004b; Scott et al., 2019). In an XROMM analysis, the bamboo shark's hyomandibulae were found to rotate substantially about their long axes, which was not found here (Scott et al., 2019). From external video, dissection and manipulation, the hyomandibulae of the lesser electric ray (*Narcine bancroftii*) were inferred to depress in a similar ventromedial direction as in *P. motoro*, but to a far greater degree, in order to facilitate the extreme protraction performance of *N. bancroftii* (Dean and Motta, 2004a). These results highlight some of the diversity of structure and function of the hyomandibulae across elasmobranchs: from the hinge-like ACHM of batoids (Dean et al., 2005) with relatively small hyomandibular depression in *P. motoro* and large depression in *N. bancroftii*, to a more rounded ACHM and large depression, protraction and long-axis rotation in the white-spotted bamboo shark (*Chiloscyllium plagiosum*).

Role of the angular cartilages

Members of the genus *Potamotrygon* exhibit diverse angular cartilage morphologies (Fontenelle et al., 2017). Angular cartilages vary in shape from gibbose to elongate, and vary in number from zero to three within the genus (Fontenelle et al., 2017). There are two angular cartilages per side in *P. motoro*, and these are moderately elongated and similar size to each other (Fig. 1). Fontenelle et al. (2017) hypothesized three functional roles of these cartilages: (1) angular cartilages extend the protractive range of the

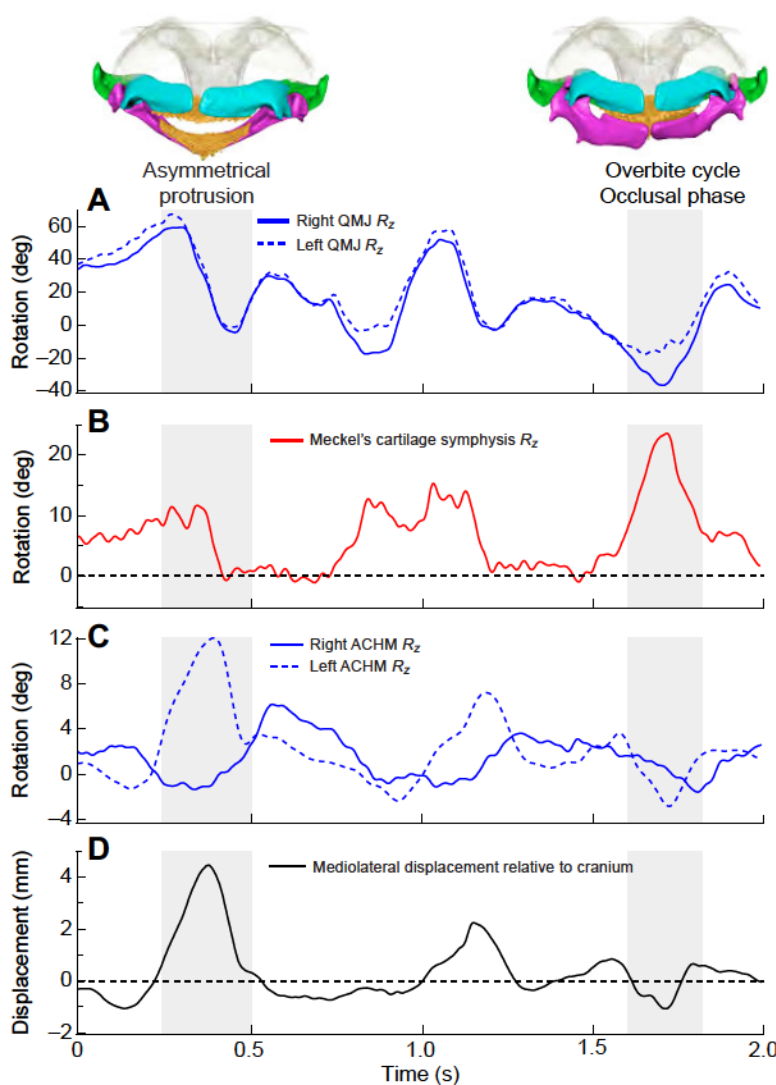


Fig. 8. Four dimensions of asymmetry are evident within a 2-s sequence of processing. (A) Differential Z-axis rotation of left and right jaw joints (JCS orientation shown in Fig. 2B) and (B) large magnitude X-axis rotation, or twisting of hemi-cartilages at the Meckel's cartilage symphysis occur during an overbite (JCS in Fig. 2C). (C) Differential Z-axis rotation of the hyomandibulae (JCS in Fig. 2A) and (D) mediolateral displacement of upper and lower jaws relative to the chondrocranium occur during protrusion.

jaws; (2) they increase the protrusive velocity of the jaws; and (3) a second angular cartilage braces and reduces motion at the hyomandibula–Meckel's cartilage joint. In comparing the difference in displacement and velocity of the lateral face of the Meckel's cartilage with the distal end of the hyomandibula, we were able to test, and support, the first and third hypotheses.

The hyomandibula-independent motion of the Meckel's cartilage landmark (Fig. 5) demonstrates that the angular cartilages add extra mobility to the hyomandibula–Meckel's cartilage joint and permit additional jaw displacement for a given hyomandibular depression. We found that during rapid jaw protrusion, the linear speed of the jaws is the same as that of the distal end of the hyomandibula. However, the direction of motion (and thus velocity) of these two landmarks are different: the distal ends of the hyomandibulae depress and come together toward the midline, whereas the jaws mainly move forward. Fontenelle and colleagues (2017) use the laws of lever mechanics to posit that longer angular cartilages increase the velocity of jaw protrusion. More kinematic data from another species with different angular cartilage lengths are needed to test the velocity hypothesis.

Our data support the bracing hypothesis. In the case of just one angular cartilage we would expect equal freedom of motion in all directions, but we found less motion in the mediolateral and

dorsoventral directions (Fig. 5B,C) than in the rostrocaudal direction (Fig. 5A), suggesting that the posterior angular cartilages may be bracing the joint and limiting these motions. However, it is also possible that muscles or ligaments may be constraining motion, and both *ex vivo* XROMM range of motion studies (Manafzadeh and Padian, 2018) and comparison with *Potamotrygon* species with just one angular cartilage are needed for further testing of the bracing hypothesis.

Overbites and kinematic modulation

Perhaps the most notable finding of this study is that *P. motoro* modulates the types of forces, both compressive and shearing, it exerts on its prey through changes in jaw motion (Fig. 6). By over-rotating the palatoquadrate during overbite cycles, the prey item is sheared between the two toothplates, rather than simply compressed, as is the case in the more frequent compressive chews. In overbite cycles, the palatoquadrate slides down over the lower toothplate in a curved, shearing motion (Fig. 6A). Overbites are associated with twisting at the symphysis between the left and right Meckel's cartilages (Fig. 6B), a more than doubling of the amount of rotation at the quadratomandibular joints (Fig. 6C), and an increase in duration of the chewing cycle. A caveat to our conclusions about prey shearing is that the toothplates of *P. motoro*

are flexible and may not move exactly with the underlying cartilages. We animated them as rigid structures moving with the cartilages, so there may be subtleties of tooth-tooth and tooth-food interactions missed by our XROMM animations. However, the overbite behavior does suggest that the homodont dentition has multiple functions. *Potamotrygon motoro* has a dentition classified as the clutching type, which consist of fields of small teeth with orally directed cusps that engage struggling prey as they attempt to escape the jaws (Cappetta, 1987). Previous studies have identified how changes in jaw position and interactions with prey can alter the positions of these teeth and result in alternate functions rather than those suggested by the morphological classification (Dean et al., 2008; Kolmann et al., 2016; Ramsay and Wilga, 2007). When clutching-type dentitions are in the typical erect position, penetration of the cusps into prey tissue is usually the result of the prey's escape attempt, yet the *P. motoro* overbite behavior lets the rays self-engage the cusps with the prey tissue. In other words, the teeth have a raking or tearing function that is gained through changes in jaw motion rather than tooth repositioning.

The overbite cycles described here may be the same shearing motions found in a prior study (Kolmann et al., 2016). However, Kolmann and colleagues report both transverse and propalinal shearing, whereas we found only evidence of the latter in our individuals feeding on beef heart and odonate larvae. It is possible that their stingrays performed behaviors not observed in the present study. Kolmann and colleagues (2016) were also able to measure changes over the duration of feeding sequences, and found that the frequency of asymmetrical motions changed throughout the duration of the feeding sequence and corresponded with prey toughness. Combining our results with those of the prior study, it appears that *P. motoro* may actively increase its use of overbites to exert shear forces on tougher prey. This behavior would necessitate rapid integration of intraoral sensory feedback; the basis of such neuromechanical function in a batoid is currently undescribed.

In addition to modulating the types of chews between crushing and shearing, *P. motoro* also modulates the relative contributions of upper and lower jaw rotation to mouth closing. In some cases, the Meckel's cartilage remained stable as the palatoquadrate rotated downwards to meet it, or vice versa. But most frequently, both the upper and lower jaws contributed to mouth closing. Interestingly, a prior study on guitarfish, another batoid, quantified the relative contribution of the upper jaw to mouth closing and found the same mean value (57%) as in the present study (Wilga and Motta, 1998). The basis of this kinematic modulation is unclear, as the jaw adductors responsible for closing the jaws attach to both the palatoquadrate and Meckel's cartilage (Miyake et al., 1992). In order to stabilize the Meckel's cartilage during a palatoquadrate-dominated chew cycle, lower jaw depressors may be isometrically active, counteracting the force from the adductors. However, this hypothesized mechanism would need to be tested by a combination of kinematics and electromyography to rule out the possibility of passive prey forces contributing to upper and lower jaw rotation modulation.

Asymmetry: passive or active?

The two major types of asymmetry observed were those related to asymmetrical hyomandibular depression, and those related to asymmetrical QMJ closing during overbites (Fig. 8). Whether these events are the result of active modulation of muscle activation patterns or the passive result of reaction forces from the prey cannot be determined conclusively without simultaneous, bilateral electromyography and XROMM. However, several factors provide compelling evidence for the hypothesis that it is active modulation.

Firstly, other elasmobranchs have been found to exhibit asynchronous muscle activity during processing (Gerry et al., 2008, 2010). Secondly, in the case of asymmetrical hyomandibular depression (Fig. 8C), the motion occurred most frequently during capture events when the prey was not contacting the jaws. Thirdly, during overbites, when asymmetry was seen in rotation at the QMJ (Fig. 8A), the side of the jaws where the prey was located sometimes closed down more. If the asymmetry were solely due to passive prey forces, we would expect the greater QMJ rotation (i.e. jaw closing) to occur consistently contralateral to the prey, but in approximately half of the cycles examined, it occurred ipsilateral to the prey. For these reasons, we find it likely that the various dimensions of asymmetry during processing are the result of active modulation. These findings reaffirm the importance of bilateral kinematic measurements in the studies of elasmobranch feeding (Gerry et al., 2010). Many of the central results of this study were enabled by the bilateral implantation of markers, and would not have been accessible through unilateral measurements.

Comparison with mammalian mastication

The processing behavior of *P. motoro* has several similarities to mammalian mastication. Both behaviors involve the combination of compressive and shear forces to break down tough prey with cyclic jaw motions, and, in both taxa, the behavior is rhythmic (low cycle duration coefficient of variation). Additionally, there is a shared element of prey manipulation and reorientation during a processing sequence. Mammals use a richly innervated tongue to move and shape the food bolus in the mouth (Hiemae et al., 1995; Montuelle et al., 2018), and *P. motoro* precisely controls water flow in and out of the mouth to manipulate prey (a 'hydrodynamic tongue' *sensu* Bemis and Lauder, 1986, and Dean et al., 2005). Unlike mammals, however, *P. motoro* shears its prey along relatively uniform occlusal surfaces, in a propalinal manner. Some mammals do engage in propalinal shearing (Hiemae, 1967); however, they translate their lower jaw forward, rather than pulling the upper jaw down.

Does *P. motoro* masticate? If mastication is defined as a synapomorphy of mammals or the result of synapomorphic mammalian morphology (Reilly et al., 2001; Ross and Iriarte-Diaz, 2014), then the answer is, by definition, no. *Potamotrygon motoro* is not a mammal, nor does it possess a temporomandibular joint and tricuspid molars. We take no position on the utility of such taxonomic characterizations of behavior. However, the present study offers compelling evidence that *P. motoro* chews its food with neuromechanical dexterity and mastication-like features that were previously thought to be absent in fish. These findings support the recent claim that *P. motoro* constitutes a model system for studying convergence on mastication-like prey processing in vertebrates (Kolmann et al., 2016). Future studies of vertebrate prey processing should continue to evaluate features that can be measured across taxa, such as CV, asymmetry and force type, as well as investigate the presumably varied sensorimotor systems that enable the behavior.

Acknowledgements

We thank M. Kolmann for animal husbandry advice, E. Tavares and E. Kaczmarek for impeccable assistance with data collection, D. Baier and S. Gatesy for XROMM MayaTools, B. Knörlein for XMALab, and K. Huffman for XMAPortal.

Competing interests

The authors declare no competing or financial interests.

Author contributions

Conceptualization: J.L., J.B.R., E.L.B.; Methodology: J.L., J.B.R., E.L.B.; Software: J.L.; Validation: J.L.; Formal analysis: J.L.; Investigation: J.L.; Resources: E.L.B.; Data curation: J.L.; Writing - original draft: J.L.; Writing - review & editing: J.L., J.B.R., E.L.B.; Visualization: J.L.; Supervision: E.L.B.; Funding acquisition: E.L.B.

Funding

The work was supported by National Science Foundation grants 1655756 and 1661129.

Data availability

The video data for this publication have been deposited in the XMAPortal (xmaportal.org) in the study 'Stingray Feeding' with permanent ID BROWN57. Video data are stored in accordance with best practices for video data management in organismal biology (Brainerd et al., 2017).

Supplementary information

Supplementary information available online at <http://jeb.biologists.org/lookup/doi/10.1242/jeb.197681.supplemental>

References

Bemis, W. E. and Lauder, G. V. (1986). Morphology and function of the feeding apparatus of the lungfish, *Lepidosiren paradoxus* (Diplopoii). *J. Morphol.* **187**, 81-108. doi:10.1002/jmor.1051870108

Brainerd, E. L., Baier, D. B., Gatesy, S. M., Hedrick, T. L., Metzger, K. A., Gilbert, S. L. and Crisco, J. J. (2010). X-ray reconstruction of moving morphology (XROMM): precision, accuracy and applications in comparative biomechanics research. *J. Exp. Zool. A. Ecol. Genet. Physiol.* **313**, 262-279. doi:10.1002/jez.589

Brainerd, E. L., Blob, R. W., Hedrick, T. L., Creamer, A. T. and Müller, U. K. (2017). Data management rubric for video data in organismal biology. *Integr. Comp. Biol.* **57**, 33-47. doi:10.1093/icb/icx060

Cappetta, H. (1987). Chondrichthyes II, mesozoic and cenozoic elasmobranchii. *Handb. Palaeoichthiol.* **3B**, 19.

Carvalho, M. R. D. E., Loboda, T. S., Paulo, J. and Silva, C. B. D. A. (2016). A new subfamily, Styracurinae, and new genus, *Styracura*, for *Himantura schmardae* (Werner, 1904) and *Himantura pacifica* (Beebe & Tee-Van, 1941) (Chondrichthyes: Myliobatiformes). *Zootaxa* **4175**, 201-221. doi:10.11646/zootaxa.4175.3.1

Crompton, A. W. and Parker, P. (1978). Evolution of the mammalian masticatory apparatus. *Am. Sci.* **66**, 192-201.

Dean, M. N. and Motta, P. J. (2004a). Anatomy and functional morphology of the feeding apparatus of the lesser electric ray, *Narcine brasiliensis* (Elasmobranchii: Batoidea). *J. Morphol.* **262**, 462-483. doi:10.1002/jmor.10245

Dean, M. N. and Motta, P. J. (2004b). Feeding behavior and kinematics of the lesser electric ray, *Narcine brasiliensis* (Elasmobranchii: Batoidea). *Zoology* **107**, 171-189. doi:10.1016/j.zool.2004.04.002

Dean, M. N., Wilga, C. D. and Summers, A. P. (2005). Eating without hands or tongue: specialization, elaboration and the evolution of prey processing mechanisms in cartilaginous fishes. *Biol. Lett.* **1**, 357-361. doi:10.1098/rsbl.2005.0319

Dean, M. N., Bizzarro, J. J. and Summers, A. P. (2007). The evolution of cranial design, diet, and feeding mechanisms in batoid fishes. *Integr. Comp. Biol.* **47**, 70-81. doi:10.1093/icb/icm034

Dean, M. N., Ramsay, J. B. and Schaefer, J. T. (2008). Tooth reorientation affects tooth function during prey processing and tooth ontogeny in the lesser electric ray, *Narcine brasiliensis*. *Zoology* **111**, 123-134. doi:10.1016/j.zool.2007.05.004

Farrell, J. H. (1956). The effect of mastication on the digestion of food. *Brit. Dent. J.* **100**, 149-155.

Fontenelle, J. P., Loboda, T. S., Kolmann, M. and Carvalho, M. R. D. E. (2017). Angular cartilage structure and variation in Neotropical freshwater stingrays (Chondrichthyes: Myliobatiformes: Potamotrygonidae), with comments on their function and evolution. *Zool. J. Linn. Soc.* **20**, 1-22. doi:10.1093/zoolinnean/zlx054

Gerry, S. P., Ramsay, J. B., Dean, M. N. and Wilga, C. D. (2008). Evolution of asynchronous motor activity in paired muscles: effects of ecology, morphology, and phylogeny. *Integr. Comp. Biol.* **48**, 272-282. doi:10.1093/icb/icn055

Gerry, S. P., Summers, A. P., Wilga, C. D. and Dean, M. N. (2010). Pairwise modulation of jaw muscle activity in two species of elasmobranchs. *J. Zool.* **281**, 282-292. doi:10.1111/j.1469-7998.2010.00703.x

Gidmark, N. J., Tarrant, J. C. and Brainerd, E. L. (2014). Convergence in morphology and masticatory function between the pharyngeal jaws of grass carp, *Ctenopharyngodon idella*, and oral jaws of amniote herbivores. *J. Exp. Biol.* **217**, 1925-1932. doi:10.1242/jeb.096248

Gintof, C., Konow, N., Ross, C. F. and Sanford, C. P. J. (2010). Rhythmic chewing with oral jaws in teleost fishes: a comparison with amniotes. *J. Exp. Biol.* **213**, 1868-1875. doi:10.1242/jeb.041012

Herring, S. W. (1993). Functional morphology of mammalian mastication. *Am. Zool.* **33**, 289-299. doi:10.1093/icb/33.3.289

Hiemae, K. M. (1967). Masticatory function in the mammals. *J. Dent. Res.* **46**, 883-893. doi:10.1177/00220345670460054601

Hiemae, K. M. (1978). Mammalian mastication: a review of the activity of the jaw muscles and the movements they produce in chewing. In *Development, Function and Evolution of Teeth*, pp. 359-398. Academic Press.

Hiemae, K. M., Hayenga, S. M. and Reese, A. (1995). Patterns of tongue and jaw movement in a cinefluorographic study of feeding in the macaque. *Arch. Oral Biol.* **40**, 229-246. doi:10.1016/0003-9969(95)98812-D

Kambic, R. E., Roberts, T. J. and Gatesy, S. M. (2014). Long-axis rotation: a missing degree of freedom in avian bipedal locomotion. *J. Exp. Biol.* **217**, 2770-2782. doi:10.1242/jeb.101428

Knölein, B. J., Baier, D. B., Gatesy, S. M., Laurence-Chasen, J. D. and Brainerd, E. L. (2016). Validation of XIMALab software for marker-based XROMM. *J. Exp. Biol.* **219**, 3701-3711. doi:10.1242/jeb.145383

Kolmann, M. A., Huber, D. R., Dean, M. N. and Grubbs, R. D. (2014). Myological variability in a decoupled skeletal system: batoid cranial anatomy. *J. Morphol.* **275**, 862-881. doi:10.1002/jmor.20263

Kolmann, M. A., Welch, K. C., Summers, A. P. and Lovejoy, N. R. (2016). Always chew your food: freshwater stingrays use mastication to process tough insect prey. *Proc. R. Soc. B Biol. Sci.* **283**, 20161392. doi:10.1098/rspb.2016.1392

Lauder, G. V. (1980). Evolution of the feeding mechanism in primitive actinopterygian fishes: a functional anatomical analysis of *Polypterus*, *Lepisosteus*, and *Amia*. *J. Morphol.* **163**, 283-317. doi:10.1002/jmor.1051630305

Lovejoy, N. R. (1996). Systematic of myliobatoid elasmobranchs: with emphasis on phylogeny and historical biogeography of Neotropical freshwater stingrays (Potamotrigonidae: Rajiformes). *Zool. J. Linn. Soc.* **117**, 207-257. doi:10.1111/j.1096-3642.1996.tb02189.x

Lucas, P. W., Prinz, J. F., Agrawal, K. R. and Bruce, I. C. (2002). Food physics and oral physiology. *Food Qual. Prefer.* **13**, 203-213. doi:10.1016/S0950-3293(00)00036-7

Luo, Z.-X. (2007). Transformation and diversification in early mammal evolution. *Nature* **450**, 1011-1019. doi:10.1038/nature06277

Maisey, J. G. (1980). An evaluation of jaw suspension in sharks. *American Museum Novitates*, no. 2706. American Museum of Natural History.

Manafzadeh, A. R. and Padian, K. (2018). ROM mapping of ligamentous constraints on avian hip mobility: implications for extinct ornithodirans. *Proc. R. Soc. B Biol. Sci.* **285**, 20180727. doi:10.1098/rspb.2018.0727

Menegaz, R. A., Baier, D. B., Metzger, K. A., Herring, S. W. and Brainerd, E. L. (2015). XROMM analysis of tooth occlusion and temporomandibular joint kinematics during feeding in juvenile miniature pigs. *J. Exp. Biol.* **218**, 2573-2584. doi:10.1242/jeb.119438

Miranda, D. L., Schwartz, J. B., Loomis, A. C., Brainerd, E. L., Fleming, B. C. and Crisco, J. J. (2011). Static and dynamic error of a biplanar videoradiography system using marker-based and markerless tracking techniques. *J. Biomech. Eng.* **133**, 121002. doi:10.1115/1.4005471

Miyake, T., McEachran, J. D. and Hall, B. K. (1992). Edgeworth's legacy of cranial muscle development with an analysis of muscles in the ventral gill arch region of batoid fishes (Chondrichthyes: Batoidea). *J. Morphol.* **212**, 213-256. doi:10.1002/jmor.1052120304

Montuelle, S. J., Olson, R. A., Curtis, H., Sidote, J. V. and Williams, S. H. (2018). The effect of unilateral lingual nerve injury on the kinematics of mastication in pigs. *Arch. Oral Biol.* **98**, 226-237. doi:10.1016/j.archoralbio.2018.11.024

Ramsay, J. B. and Wilga, C. D. (2007). Morphology and mechanics of the teeth and jaws of white-spotted bamboo sharks (*Chiloscyllium plagiosum*). *J. Morphol.* **268**, 254-274. doi:10.1002/jmor.10530

Reilly, S. M., McBrayer, L. D. and White, T. D. (2001). Prey processing in amniotes: biomechanical and behavioral patterns of food reduction. *Comp. Biochem. Physiol. A Mol. Integr. Physiol.* **128**, 397-415. doi:10.1016/S1095-6433(00)00326-3

Ross, C. F. and Iriarte-Diaz, J. (2014). What does feeding system morphology tell us about feeding? *Evol. Anthropol.* **23**, 105-120. doi:10.1002/evan.21410

Ross, C. F., Eckhardt, A., Herrel, A., Hylander, W. L., Metzger, K. A., Schaeilaeken, V., Washington, R. L. and Williams, S. H. (2007). Modulation of intra-oral processing in mammals and lepidosaurs. *Integr. Comp. Biol.* **47**, 118-136. doi:10.1093/icb/icm044

Sasko, D. E., Dean, M. N., Motta, P. J. and Hueter, R. E. (2006). Prey capture behavior and kinematics of the Atlantic cownose ray, *Rhinoptera bonasus*. *Zoology* **109**, 171-181. doi:10.1016/j.zool.2005.12.005

Scott, B., Wilga, C. A. and Brainerd, E. L. (2019). Skeletal kinematics of the hyoid arch in the suction-feeding shark *Chiloscyllium plagiosum*. *J. Exp. Biol.* **222**, doi:10.1242/jeb.193573

Sokal, R. R. and Rohlf, F. J. (1981). Biostatistics: principles and applications. W.H. Freeman and Company, San Francisco.

Turnbull, W. D. (1970). Mammalian masticatory apparatus. *Fieldiana Geol.* **18**, 149-356.

Wilga, C. D. (2002). A functional analysis of jaw suspension in elasmobranchs. *Biol. J. Linn. Soc.* **75**, 483-502. doi:10.1046/j.1095-8312.2002.00037.x

Wilga, C. D. and Motta, P. J. (1998). Feeding mechanism of the Atlantic guitarfish *Rhinobatos lentiginosus*: modulation of kinematic and motor activity. *J. Exp. Biol.* **201**, 3167-3184.

Table S1. Principal component loadings from analysis of joint rotations

Kinematic Variables		PC1 74.42%	PC2 8.15%	PC3 5.66%	PC4 2.93%
		Component Loadings			
Right QMJ	R_x	0.054	-0.084	0.111	-0.021
	R_y	0.121	-0.287	0.097	-0.466
	R_z	0.660	0.727	-0.009	-0.124
Left QMJ	R_x	0.065	-0.118	0.106	-0.025
	R_y	0.107	-0.059	0.186	-0.470
	R_z	0.672	-0.570	-0.363	0.076
Meckel's cartilage symphysis	R_x	0.141	-0.091	0.012	0.504
	R_y	0.137	-0.037	0.444	0.230
	R_z	0.113	-0.042	0.290	0.034
Palatoquadrate symphysis	R_x	0.070	0.050	0.090	0.481
	R_y	0.094	-0.121	0.597	0.012
	R_z	0.123	-0.108	0.393	-0.008

Motions are defined by JCS orientation depicted in Figures 1 and 2.

Table S2. Results of precision study

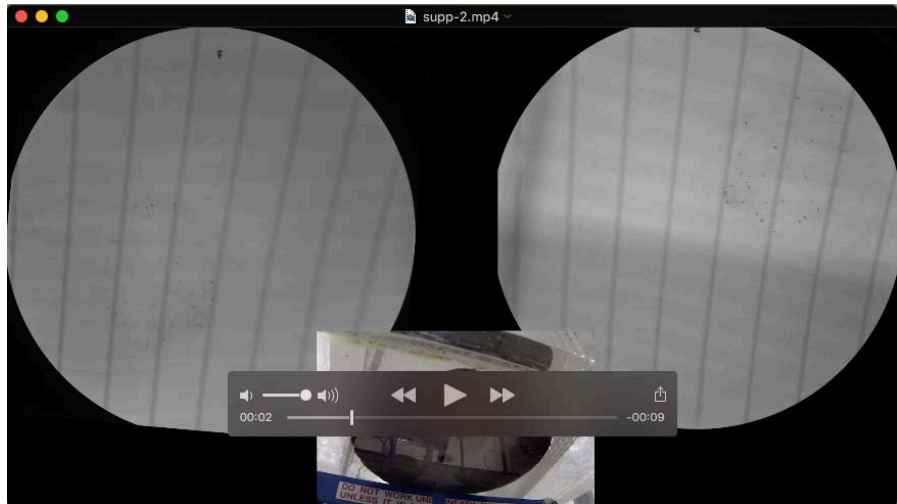
Element	T _x	T _y	T _z	R _x	R _y	R _z
	Precision Threshold (mm)			Precision Threshold (deg)		
Right QMJ	0.076	0.102	0.064	0.263	0.402	0.638
Left QMJ	0.129	0.133	0.066	0.214	0.485	0.916
Meckel's cartilage symphysis	0.019	0.083	0.038	0.728	0.264	0.461
Palatoquadrata symphysis	0.022	0.054	0.039	0.824	0.394	0.331
Right ACHM	0.018	0.019	0.060	0.490	0.781	0.160
Left ACHM	0.103	0.125	0.204	0.805	0.603	0.225
AAC attachment site on right hyomandibula	0.038	0.042	0.069	-	-	-
AAC attachment site on left hyomandibula	0.083	0.083	0.147	-	-	-
AAC attachment site on right Meckel's cartilage	0.075	0.065	0.098	-	-	-
AAC attachment site on left Meckel's cartilage	0.068	0.046	0.089	-	-	-

No rotations are given for the AAC attachment sites, as only the displacement of the distal hyomandibula and lateral face of the Meckel's cartilage were measured.

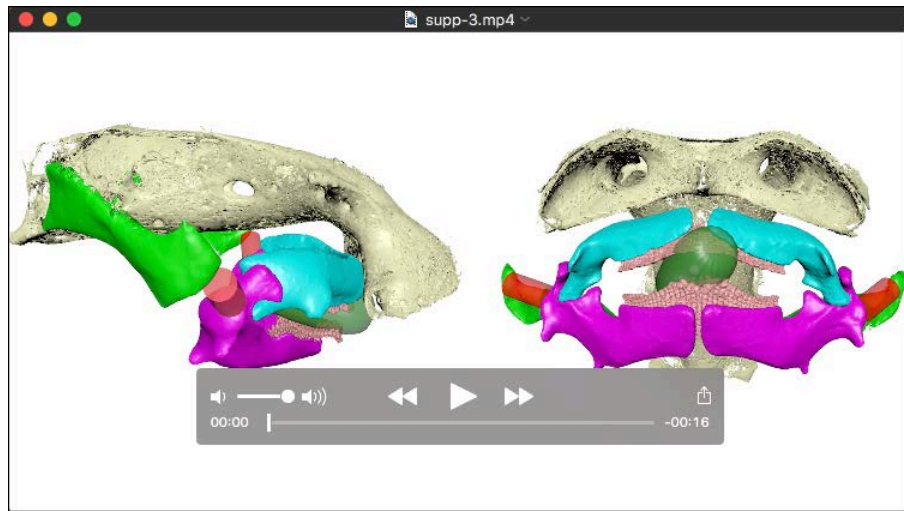
Table S3. Per-cycle joint rotation means calculated two ways

Joint	Degree of Freedom					
	R _x		R _y		R _z	
	PI	PD	PI	PD	PI	PD
QMJ	0.41 ± 1.71	5.33 ± 2.08	6.68 ± 2.68	10.34 ± 3.02	-33.99 ± 9.20	36.09 ± 9.62
ACHM	0.06 ± 0.65	2.08 ± 1.05	0.16 ± 0.40	1.78 ± 1.00	0.06 ± 1.84	3.02 ± 1.57
MC Symphysis	0.14 ± 3.60	12.81 ± 4.67	2.82 ± 4.34	11.22 ± 3.9	2.00 ± 3.03	10.30 ± 3.28
PQ Symphysis	2.84 ± 2.82	12.80 ± 3.93	-2.21 ± 4.23	10.75 ± 4.15	-0.71 ± 3.73	9.59 ± 3.52

PI, path independent; PD, path dependent. See methods for description of calculation methods. All values are mean ± s.e.m.



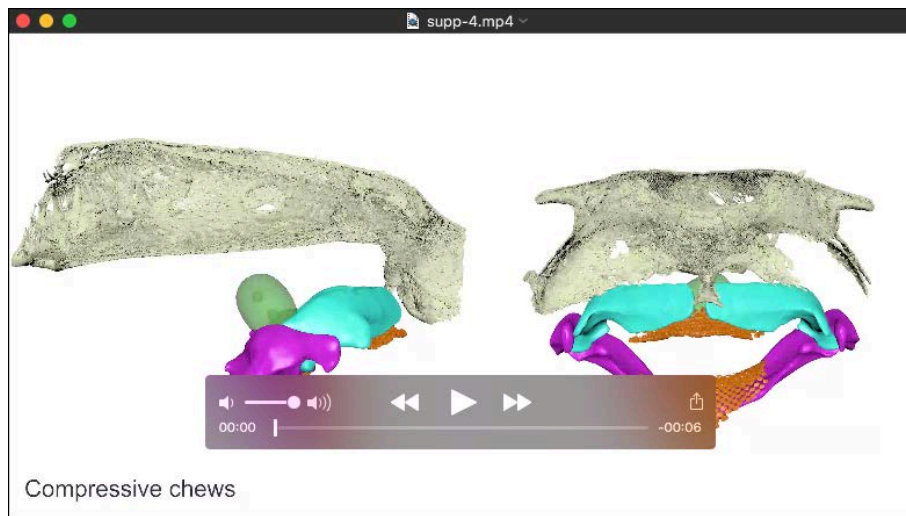
Movie 1. Example trial of unprocessed X-ray and light video data. X-ray cameras were positioned at oblique dorsoventral angles and recorded 10 s sequences. A GoPro (bottom panel) recorded continuously to capture the full duration of the feeding sequence.



Movie 2. XROMM animation of *P. motoro* feeding. Left, right lateral view; right, rostroventral view.

Two beads in the prey item allowed us to reconstruct prey position and orientation (green solid).

Angular cartilages (red cylinders) were animated based on the motion of proximal and distal attachment sites on the hyomandibula and Meckel's cartilage, respectively.



Movie 3. Comparison of overbite and compressive chews. Left, right lateral view; right, rostral view. In compressive chews, the toothplates (orange) do not pass the expected occlusal limit, whereas in overbite chews, the upper jaw toothplates shear down past the lower jaw.